

Charge inversion at minute electrolyte concentrations

J. P. Ittler,¹ W. Bu,² D. Vaknin,² A. Travasset,² D. J. McGillivray,³ and M. Losche³

¹Institute of Experimental Physics I, University of Leipzig, D-04103 Leipzig, Germany;

²Ames Laboratory and Department of Physics and Astronomy, Iowa State University, Ames, Iowa 50011;

³CNBT Consortium, NIST Center for Neutron Research, Gaithersburg, MD 20899

and Department of Physics, Carnegie Mellon University, Pittsburgh, PA 15213

(Dated: May 4, 2021)

Anionic DMPA monolayers spread on LaCl_3 solutions reveal strong cation adsorption and a sharp transition to surface overcharging at unexpectedly low bulk salt concentrations. We determine the surface accumulation of La^{3+} with anomalous x-ray reactivity and find that La^{3+} compensates the lipid surface charge by forming a Stern layer with 1 La^{3+} ion per 3 lipids below a critical bulk concentration, $c_c \approx 500 \text{ nM}$. Above c_c , the surface concentration of La^{3+} increases to a saturation level with 1 La^{3+} per lipid, thus implying that the total electric charge of the La^{3+} exceeds the surface charge. This overcharge is observed at 4 orders of magnitude lower concentration than predicted in ion-ion correlation theories. We suggest that transverse electrostatic correlations between mobile ions and surface charges (interfacial Bjerrum pairing) may account for the charge inversion observed in this dilute regime.

PACS numbers: 73.30.+y, 82.45.Mp

Counterion screening of charged interfaces in electrolytic solutions is key for understanding a broad range of phenomena in molecular biology, colloid and polymer science, or microfluidics. Directly or indirectly, charges at cell membrane surfaces control functions and conformations of nearby molecules that may be involved in inter- and intracellular transport processes, cell-cell recognition and biomimetic mineralization processes. Despite extensive experimental and theoretical work performed over more than a century, problems regarding the nature of ion correlations, the role of the hydration sheath in physical processes and the structure of water near charged interfaces remain the subject of intense theoretical and experimental work [1, 2, 3].

The phenomenology of the electrostatics in soft media is rich and complex. Effects such as charge inversion, where charges at an interface attract counterions in excess of their own nominal charge density have been reported in the literature [1, 2, 4, 5, 6]. Current theories assume that charge inversion results from the free energy gain brought about by ion-ion correlations [1] and predict that measurable charge inversion occurs when $q = \left(\frac{\sigma}{\epsilon_0}\right)^{-1} > 1$, where $q = Ze$ is the counter-ion charge and σ is the surface charge density. $\lambda_D = \left(\frac{\epsilon_0 \epsilon}{8 \pi I}\right)^{1/2}$ is the Debye length of an electrolytic solution (Bjerrum length, $\lambda_B = e^2 / (k_B T)$) with ionic strength I [7]. Applying this reasoning to Langmuir films of a charged lipid such as phosphatidic acid, one expects for a typical area per amphiphile, $A_{\text{lipid}} (= e =) \approx 40 \text{ \AA}^2$, spread on LaCl_3 solution ($Z = 3$), that the salt concentration has to be at least in the 10 mM range for charge inversion to become significant. Besides correlations of the mobile ions, there are other effects that may contribute to the phenomenon. For example, it has recently been suggested that transverse correlations, i.e., correlations between interfacial charges and mobile ions, may also play a role in the generation of charge inversion [8, 9].

In this paper, we demonstrate charge inversion at ultra-low (M or less) LaCl_3 electrolyte concentrations with surface-sensitive, resonant X-ray scattering at the La L_{III} absorption edge and discuss its relationship to proton transfer and release. These results extend previous studies of BaCl_2 [10, 11] and CsI solutions [12, 13].

Surface monolayers of DMPA (1,2-dimyristoyl-sn-glycero-3-phosphatidic acid) (A vantipolar Lipids), were spread from chloroform/methanol (3:1; both from Merck, p.a. grade) on aqueous solutions with different LaCl_3 (Sigma, purity: $> 99\%$) solutions prepared from ultrapure water (NANOpure, Bamstead) in an enclosed Teon (PTFE) Langmuir trough. For the x-ray scattering work, the air space above the trough was continuously purged with water-saturated helium. Both isotherm and scattering studies were performed at a temperature of $21 \text{ }^\circ\text{C}$. To minimize ion contamination, the subphases were handled and transferred to the Langmuir film balance in bottles made from Teon (Fisher Scientific). After solvent evaporation, the monolayers were compressed at a rate of $1 \text{ \AA}^2 = (\text{molecule min.})$ to record isotherms or measure reactivities at various surface pressures between $\sigma = 10$ and 50 mN/m . At bulk ion concentrations in the M range, monolayers become progressively unstable to compression. At a collapse pressure, σ_c , the compressibility of the surface film increases, consistent with a gradual transformation of the monolayer locally into bilayer or trilayer structures. σ_c decreases with increasing salt concentration, which makes measurements at high difficult for $c_{\text{bulk}}^{\text{LaCl}_3} > 1 \text{ M}$. We restrict the following discussion to the low surface pressure regime, $\sigma = 15 \text{ } :: 30 \text{ mN/m}$.

X-ray reactivity (XR) measurements were conducted on the Ames Laboratory horizontal surface diffractometer at beam line 6-ID-B of the Advanced Photon Source (APS). The highly monochromatic beam (energy resolution, $E = 1 \text{ eV}$), selected by an initial Si double crys-

tal monochromator, is detected onto the liquid surface at a specified incidence angle by a secondary Ge(111) monochromator located at the diffractometer [14]. The x-ray energy E was calibrated by measuring the absorption spectrum of a dilute LaCl_3 solution. On-resonance spectra were measured at 8.0 keV, and "on-resonance" refers to the La L_{III} edge at $E_{\text{res}} = 5.486 \text{ keV}$. To reduce radiation damage, the Langmuir trough was periodically translated across the beam. To monitor sensitively for damage, in particular after prolonged exposure of the sample at high momentum transfer, Q_z , measurements were routinely repeated (without translating the sample) across the Q_z regions of the sharp cusps in the interference minima.

To extract scattering length density (SLD) distributions across the interface from the XR data, parameterized profiles $\rho(z) = \rho^0(z) + i\rho^{\text{im}}(z)$ were constructed in which the real and imaginary parts of ρ describe the electron density (ED) and the absorption density (AD), respectively, along the surface normal, z . We used both a modified 'box' model approach [13, 15] and the quasi-molecular Volume-Restricted Distribution Function (VRDF) approach [11, 16] for this reconstruction to obtain stable results and to check for consistency. In the box model, $\rho(z)$ is described by a sum of error functions

$$\rho(z) = \frac{1}{2} \sum_{j=1}^N \text{Erf} \left[\frac{z - z_j}{\frac{z_j - z_{j+1}}{2}} \right] \quad (j = j+1) + \frac{N+1}{2} \quad (1)$$

where N is the total number of slabs j that describe the monolayer. z_j and $\frac{z_j - z_{j+1}}{2}$ denote the position and rms roughness of the j th interface, respectively, between the slabs, and $j = N + 1$ indicates the bulk subphase. Alternatively, $\rho(z)$ is constructed from a sequence of themally broadened distributions, modeled as Gaussian functions, that represent parsed subfragments of the lipid structure and bound cations [10, 11]. In both approaches, volume filling is implemented by accounting for the subfragment volumes as derived from molecular dynamics simulations [17]. For either model, $\rho^{\text{im}}(z)$ is only significant in spectra measured at E_{res} and correlates with the physical distribution of the cations across the interface, i.e., it is negligible where the cation density is at bulk density or below. Reflectivities are calculated from $\rho(z)$ by applying a recursive method [18] to the discretized profiles. Both $\rho^0(z)$ and $\rho^{\text{im}}(z)$ are calculated from $\rho(z)$ by applying a recursive method [18] to the discretized profiles. Both $\rho^0(z)$ and $\rho^{\text{im}}(z)$ are calculated from $\rho(z)$ by applying a recursive method [18] to the discretized profiles. Both $\rho^0(z)$ and $\rho^{\text{im}}(z)$ are calculated from $\rho(z)$ by applying a recursive method [18] to the discretized profiles.

$$n_{\text{La}^{3+}} = \frac{R^{\text{im}}}{z_e A_{\text{lipid}}} \quad (2)$$

where $z_e = 19.0$ is the difference between the effective numbers of electrons for La^{3+} at $E_{\text{on-res}}$ and E_{res} .

Figure 1 shows isotherms, π , vs. A_{lipid} , of DM PA monolayers at various LaCl_3 concentrations of the bulk subphase. On the salt-free subphase, a sloped plateau indicates coexistence of a liquid and a hexatic lipid phase.

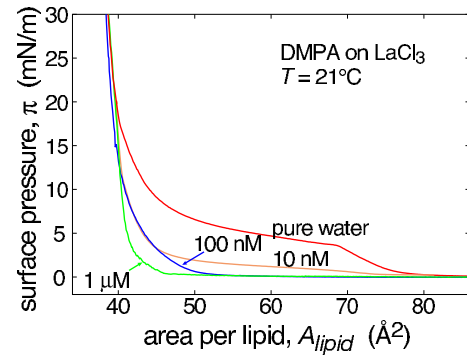


FIG. 1: DMPA monolayer isotherms for different La^{3+} sub-phase concentrations

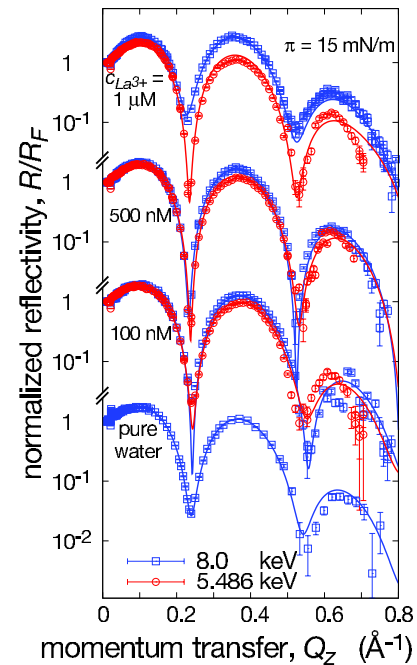


FIG. 2: Fresnel-normalized x-ray reflectivities, R/R_F , of DMPA monolayers at $E = 8.0 \text{ keV}$ (on-resonance) and 5.486 keV (La L_{III} resonance) on aqueous LaCl_3 solutions. For clarity, subsequent pairs of data sets are offset by a factor of 100 each. Solid lines derive from model fits.

The height of this plateau depends sensitively on salt concentration. As shown earlier, micromolar concentrations of Ca^{2+} condense the monolayer to the extent that this plateau disappears [19]. Figure 1 shows that trivalent cations are even more effective in monolayer condensation and the plateau has already been lost at $C_{\text{bulk}}^{\text{LaCl}_3} > 10 \text{ nM}$, consistent with strong electrostatic interactions between La^{3+} and the DM PA headgroups. It has been shown with fluorescence microscopy that Ca^{2+} condenses DM PA from the two-dimensional (2D) gas phase into hexatic domains [19]. We expect that binding of La^{3+} to DM PA has a similar effect already at exceedingly low salt concentrations.

Figure 2 shows exemplary, Fresnel-normalized on-

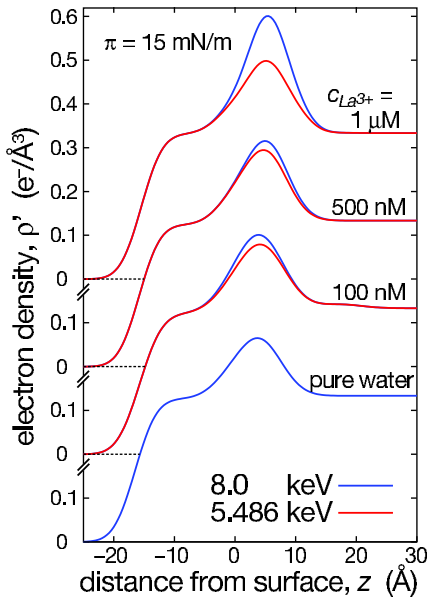


FIG. 3: VRDF electron density profiles derived from fits to the experimental data. The off-resonance and on-resonance data shown in Fig. 2 were correlated with consistent sets of parameters that deviated only in the effective electron numbers and absorption cross sections of the La^{3+} component. Subsequent ED pairs are offset by $0.2 \text{ e}^-/\text{\AA}^3$ for clarity. Similar ED profiles were derived from a modified box model as described in the text. The number density of La^{3+} at the interface was subsequently obtained from such models via Eq. 2.

off-resonance/on-resonance reactivity pairs of DMPA monolayers at $\pi = 15 \text{ mN/m}$ on subphases that contain 100, 500, and 1 M LaCl_3 . A high-energy reactivity of DMPA on pure water is also shown. Qualitatively, the increase in intensity with increasing LaCl_3 bulk concentration indicates ED increases due to the accumulation of La^{3+} at the acidic interfaces. Quantitatively, the difference between off-resonance and on-resonance EDs is proportional to the La^{3+} surface concentration (Eq. 2). The data fall in two categories: Between $c_{\text{bulk}}^{\text{LaCl}_3} = 0$ and 500 nM LaCl_3 , both off-resonance and resonance reactivities are rather similar. Above 500 nM LaCl_3 , on the other hand, the off-resonance reactivities are significantly higher at all Q_z than those at resonance. Without any model interpretation, this qualitative difference shows conclusively that the condensation of La^{3+} at the monolayer is significantly larger at 1 M LaCl_3 than at 500 nM and below. This is corroborated and quantified by a detailed data analysis (see Fig. 3), using the modified box model and the VRDF. We also measured more complete, systematic sets of off-resonance reactivities over a wider range of subphase salt concentrations, between 100 nM and 10 M, and at higher surface pressures. As shown in Fig. 4, these results are consistent with the more stringent anomalous reactivity data.

Figure 3 shows SLD profiles $\rho(z)$ obtained from a correlation of data pairs shown in Fig. 2. While $\rho(z)$ in the lipid headgroup region is larger for the off-

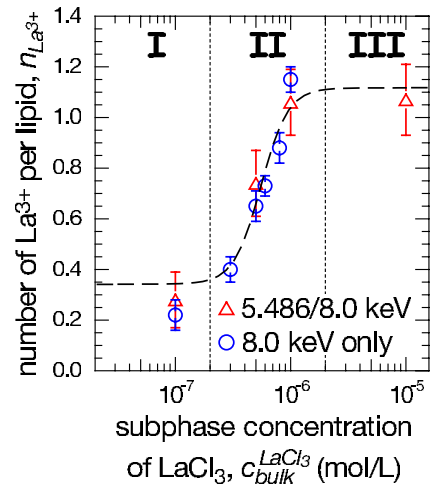


FIG. 4: Number of adsorbed La^{3+} per DMPA in surface monolayers as a function of bulk LaCl_3 concentration. Red plot symbols indicate results at 15 mN/m derived from the anomalous reactivity data pairs shown in Fig. 2 and ED profiles similar to those shown in Fig. 3. The results indicated by blue symbols were derived from independent data measured at 8.0 keV alone.

resonance data than for the on-resonance data on all LaCl_3 -containing subphases, the difference is much larger for 1 M LaCl_3 . The VRDF modeling suggests that the differences in $\rho(z)$, to be interpreted as the distribution of cations at the interface, are connected to the lipid headgroup region. Equation 2 serves to determine $n_{\text{La}^{3+}}$, the number of La^{3+} per DMPA headgroup in the monolayer. A compilation of this data collected at various surface pressures as a function of $c_{\text{bulk}}^{\text{LaCl}_3}$, is given in Fig. 4. The plot shows clearly three distinct regimes which consist of two plateaus at low and high $c_{\text{bulk}}^{\text{LaCl}_3}$, separated by a sharp transition. In regime I, between 100 nM and 200 nM LaCl_3 , $n_{\text{La}^{3+}}$ is constant at 0.34 ± 0.1 . It is followed by a remarkably sharp transition, regime II, that connects this regime with regime III, observed at high LaCl_3 concentration ($> 1 \text{ M}$), where $n_{\text{La}^{3+}} \approx 1$.

The results in regime I correspond to 1 La^{3+} bound to three DMPA at the interface. This stoichiometry follows from the dissociation constants of the first and second protons to DMPA, $\text{p}K_{a,1} = 2.1$ and $\text{p}K_{a,2} = 7.1$ [21], and the binding constant of La^{3+} to a monovalent phosphate group, estimated as $K_B \approx 100 \text{ M}^{-1}$ [9], introduced into the PB theory [9, 20]. Regime II follows from the large affinity of La^{3+} ions to divalent phosphate groups at the interface, $K_B \approx 10^5 \text{ M}^{-1}$ [9], which leads to deprotonation, $\text{PO}_4\text{H} \rightleftharpoons \text{PO}_4^-$, of the interfacial group at a concentration $c_{\text{bulk}}^{\text{La}^{3+}} \approx 10^6$. The increase of $n_{\text{La}^{3+}}$ from $1/3$ to $2/3$ is therefore not due to charge inversion, but rather to a doubling of interfacial charge density by surface deprotonation. Regime III with $n_{\text{La}^{3+}} \approx 1$, on the other hand, clearly shows charge inversion that is not covered by established ion-ion correlation theories [1]. The experimental observation of charge inversion in this

concentration range is thus compelling evidence for yet other effects of the interface [9]. A hypothetical Stern layer, that would consist of La^{3+} bound to interfacial PO_4^{2-} in a 1:1 ratio ($n_{\text{La}^{3+}} = 1$), leads inevitably to a diffuse distribution of co-ions (e.g., Cl^-) which results in a free energy penalty (per amphiphile) of [7]

$$F = 2 \left(\ln \left(\frac{p}{2} \right) - \frac{p}{2} \right) \frac{1}{D = G_C} \approx 18 k_B T; \quad (3)$$

where $G_C = e(2 \lambda_B)$ is the Gouy-Chapman length. We envisage two scenarios, under which such a free energy penalty could be compensated by other effects: (1) A "molten salt" state consisting La^{3+} ions intercalated between the negative charges on the phosphate oxygens forming a highly correlated state [9]. (2) Enhanced adsorption in the Stern layer via non-electrostatic interactions, for example, hydrogen bonding between the PO_4^{2-} oxygens (acceptor) and a $\text{La}(\text{OH})^{2+}$ complex (donor). In either scenario, charge inversion is associated with some instability of the Langmuir monolayer, as evidenced by slow collapse at intermediate surface pressures at LaCl_3 concentrations above $5 \times 10^5 \text{ M}$.

In this paper we presented experimental evidence for charge inversion at minute electrolyte concentrations ($0.5 \text{ M } \text{LaCl}_3$) in contact with acidic DMPC monolayers. When compared with experimental work investigating forces between charged plates [6], charge inversion in our experiment is observed at 2 orders of magnitude lower and in the absence of any monovalent salt. More fundamentally, our results provide strong indication that correlations among mobile ions and interfacial charges play a prominent role in the generation of charge

inversion. We interpret the concentration dependence of counter-ion accumulation beyond regime (I) in Fig. 4 as follows: Charge inversion is initiated by the deprotonation of the secondary oxygen in the phosphate group (regime II). The high level of charge inversion at M bulk LaCl_3 (regime III) requires additional effects of ion reorganization, and we suggested two tentative scenarios.

The results presented in this study corroborate the notion that charge inversion is a generic effect for multivalent ions next to highly charged surfaces and quantify the role of multivalent ions in favoring surface deprotonation. Furthermore, however, these results are likely of universal relevance for the physics of highly charged colloidal or biological systems in the presence of multivalent ions, as evidenced from previous studies [4, 10]. Finally, it is also clear that still more experimental and theoretical work is needed to fully resolve the fundamental issues involved in the electrostatics of highly charged interfaces.

We thank D. S. Robinson and D. Wermille for technical support at the 6-ID beam line, and to J. Faraudo for helpful discussions. The MUCAT sector at the APS is supported by the U.S. DOE, Basic Energy Sciences, Office of Science, through Ames Laboratory under contract No. W-7405-Eng-82. Use of the Advanced Photon Source is supported by the U.S. DOE, Basic Energy Sciences, Office of Science, under Contract No. W-31-109-Eng-38. ML was supported by the NSF (grant no. 0555201), the NIH (grant no. 1R01RR14812), the Regents of the University of California, and the Volkswagen Foundation (grant no. I/77709). AT is partially supported by NSF-DMR-0426597.

-
- [1] A.Yu. Grosberg, T.T. Nguyen, and B.I. Shklovskii, *Rev. Mod. Phys.* 74, 329 (2002).
- [2] H. Boroudjerdi, Y.-W. Kim, A. Najji, R.R. Netz, X. Schlagberger and A. Serr, *Phys. Rep.* 416, 129 (2005).
- [3] Y. Levin, *Rep. Prog. Phys.* 65, 1577 (2002).
- [4] S. Mclaughlin, *Annu. Rev. Biophys. Chem.* 18, 113 (1989).
- [5] K. Besteman, M.A.G. Zevenbergen, H.A. Heering and S.G. Lemay, *Phys. Rev. Letters* 93, 170802 (2004).
- [6] K. Besteman, M.A.G. Zevenbergen and S.G. Lemay, *Phys. Rev. E* 72, 061501 (2005).
- [7] S. Safran, *Statistical Thermodynamics of Surfaces, Interfaces, and Membranes*, *Frontiers in Physics*, Perseus Publishing, 1994.
- [8] M.L. Henle, C.D. Santangelo, D.M. Patel, P.A. Pincus, *Europhys. Letters* 66, 284 (2004).
- [9] A. Travesset and D. Vaknin, *Europhys. Lett.* 74, 181 (2006).
- [10] D. Vaknin, P. Knüger and M. Losche, *Phys. Rev. Letters* 90, 178102 (2003).
- [11] M. Schalke, P. Knüger, M. Weygand and M. Losche, *Biochim. Biophys. Acta* 1464, 113 (2000).
- [12] W. Bu, D. Vaknin, A. Travesset, *Phys. Rev. E* 72, 060501(R) (2005).
- [13] W. Bu, D. Vaknin, A. Travesset, *Langmuir* 22, 5673 (2006).
- [14] D. Vaknin, in *Methods in Materials Research*, E.N. Kaufmann, et al., Eds., John Wiley & Sons, New York, pp. 10d.2.1 (2001).
- [15] J. Als-Nielsen and K. Kjær, in *Phase Transition in Soft Condensed Matter*, T. Riste and D. Sherrington, Eds., Plenum Press, New York, 113 (1989).
- [16] M. Schalke and M. Losche, *Adv. Colloid Interf. Sci.* 88, 243 (2000).
- [17] R.S. Ammen, O.D. Uitto and S.E. Feller, *Biophys. J.* 75, 734 (1998).
- [18] L.G. Parratt, *Phys. Rev.* 95, 359 (1954).
- [19] M. Losche and H. Mohwald, *J. Colloid Interf. Sci.* 131, 56 (1989).
- [20] J.N. Israelachvili, *Intermolecular and Surface Forces*, Academic Press, London, 2000.
- [21] P. Atkins and J. de Paula, *Physical Chemistry*, W.H. Freeman & Co., New York, 2001.